

# Chromium Oxide – A Novel Sacrificial Layer Material for MEMS/NEMS and Micro/Nanofluidic Device Fabrication

Alokik Kanwal, B. Robert Ilic, Christopher H. Ray, Kerry Seibein, and J. Alexander Liddle

## Abstract

Free standing membranes for fluidic devices typically require long etching times due to the slow, diffusion limited exchange of etchant and etch products when large etch distances are involved. In these cases, high etch selectivity is required between the sacrificial and channel-wall materials. Here, we introduce chromium oxide,  $\text{Cr}_2\text{O}_3$ , as a versatile sacrificial layer material for the fabrication of microfluidic and nanofluidic channels. Chromium oxide has many desirable attributes as a sacrificial layer: it can be deposited by sputtering to form stress-controlled films, it adheres well to both metal and dielectric surfaces, it is resistant to most acids and bases, but etches rapidly in standard chromium etchants, and has minimal tendencies to react with other commonly used materials. In addition, typical chromium etchants are highly selective to materials commonly used in microfabricated systems. To fully explore the process characteristics of this material we performed a comprehensive set of experiments to quantify its behavior in ways relevant to its use in device fabrication. The results presented in this paper will provide a starting point to optimize  $\text{Cr}_2\text{O}_3$  for fabrication of fluidic devices.

## Keywords

Microfluidics  
Nanofluidics  
Sacrificial Etch  
Membranes  
MEMS  
NEMS

## 1. Introduction

Sacrificial layer etching is a well-developed method for producing free-standing membranes or micro- and nanofluidic channels in a wide variety of materials.[1, 3] However, for fluidic devices, the production of complex, fully enclosed systems typically requires long etching times due to the slow, diffusion limited exchange of etchant and etch products when large etch distances are involved. In these cases, high etch selectivity is required between the sacrificial and channel-wall materials. This constraint is even more demanding when the thickness of the channel walls is limited. The same is true when very thin or large aspect ratio membranes are needed.[2, 4]

Recently, we developed a novel nanofluidic cell that enables high-resolution electron microscopy in liquids. This device requires the formation of long nanofluidic channels between thin silicon nitride membranes, making good etch selectivity paramount. Our initial fabrication process employed amorphous silicon as the sacrificial material. Despite the excellent etch selectivity between silicon and silicon nitride in potassium hydroxide, the lateral etch distance was great enough to result in significant loss of silicon nitride and the inability to develop a reproducible and robust device fabrication process. This problem motivated the search for an alternative sacrificial layer material.

Here, we introduce  $\text{Cr}_2\text{O}_3$  as a versatile sacrificial layer material for the fabrication of microfluidic and nanofluidic channels in lab-on-a-chip applications. [5] While chromium metal can serve as an effective sacrificial material,[6] chromium oxide possesses additional attributes that make it particularly useful: it can be readily deposited by sputtering to form stress-controlled films several hundred nanometers thick, it adheres well to both metal and dielectric surfaces, it is resistant to most acids and bases, but etches rapidly in standard chromium etchants, and, since it is a stable oxide,[7] it has minimal tendencies to react with other commonly-used materials, both metals and dielectrics, even at high temperatures. This latter characteristic makes it useful for encapsulating and protecting, for example, metal electrodes during a high-temperature low-pressure chemical vapor deposition step. In addition, the standard ceric ammonium nitrate etchant does not attack many of the materials commonly used in microfabricated systems to any measurable degree.[8]

In order to fully explore the process characteristics of this material, we have carried out a series of experiments designed to quantify its behavior in ways relevant to its use in device fabrication. We present the results of those experiments here.

## 2. Material Deposition

The chromium oxide thin films examined in this study were deposited from a 99.9% pure chromium oxide target ( $\text{Cr}_2\text{O}_3$ ) by RF magnetron sputtering, using Ar as the working gas, onto (100), 100 mm diameter Si substrates. In order to avoid damage to the target, the power was increased in steps prior to deposition. Films were deposited at thicknesses of approximately 200 nm, unless otherwise specified. Film thicknesses were measured using ellipsometry and fitted using the Tauc-Lorentz model. Stress measurements were performed with an instrument which used a laser reflectometer to measure the radius of curvature of each wafer before and after film deposition and calculated the stress based on the change. The same instrument was used to measure stress versus temperature. The temperature was computer controlled and held at each measurement point while a stress measurement was made. X-ray diffractometry (XRD) measurements were performed in vacuum using a heated stage with a graphite dome over the wafer to ensure temperature uniformity. The ramp rate for the temperature was 35°C per minute. The temperature was held constant for 3 minutes prior to a scan. Atomic force microscope (AFM) measurements were taken in non-contact mode. The etchant and chemicals used were complementary metal oxide semiconductor (CMOS) grade.

### 3. Results

#### 3.1. Stress

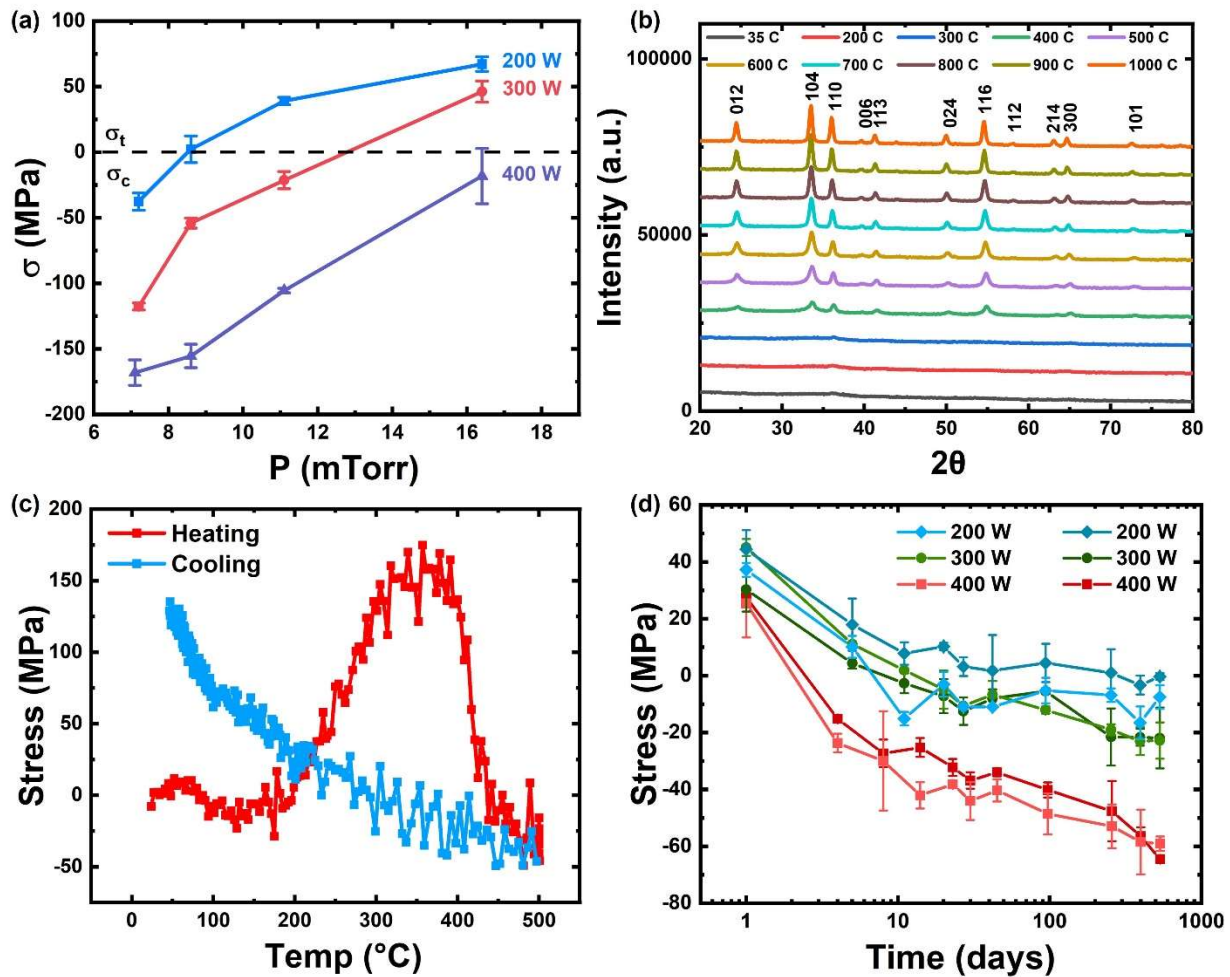


Figure 1. (a) Chromium oxide film stress ( $> 0$  MPa is tensile) as a function of working gas [Ar] pressure, for magnetron sputter deposition at powers of 200 W (blue squares), 300 W (red circles), and 400 W (purple triangles). The error bars represent  $\pm$  one standard deviation. The stress can be readily controlled over the range about zero. (b)  $2\theta$  x-ray diffraction data for 209 nm thick chromium oxide film deposited at 400 W and  $\approx 2$  Pa (17.6 mTorr) working gas pressure. These settings were chosen as they are closest to zero stress which is of great interest for membranes. Each trace is taken at a different temperature, as indicated by the legend. The traces are offset for clarity. The peaks are consistent with  $\text{Cr}_2\text{O}_3$ , as indicated. The film crystallinity increases with annealing temperature. (c) Plot of film stress as a function of temperature for a 205 nm thick chromium oxide film deposited using  $\approx 2$  Pa (17 mTorr) Ar working gas pressure, and at a power of 400 W. Note the dramatic change in stress that coincides with the first signs of crystallization seen in figure 1(b). (d) Time series measurements of the stress in as-deposited films held at room temperature showing long-term stress changes. The films were deposited at  $\approx 1$  Pa (7 mTorr). The error bars represent  $\pm$  one standard deviation of multiple measurements.

As deposited, the material is amorphous, but it undergoes significant crystallization at temperatures above approximately 400 °C. As shown by the amplitude of the peaks in the  $2\theta$  x-ray diffraction data (Figure 1(b)), the degree of crystallinity becomes more pronounced as the annealing temperature is increased. The diffraction data are consistent with the material having the structure of  $\text{Cr}_2\text{O}_3$  [11, 12]

The crystallization threshold temperature is also reflected in the plot of stress versus temperature, shown in Figure 1(c). Interestingly, the stress remains constant and compressive until about 200 °C, before

becoming tensile. This is counter to what would be expected from the thermal expansion mismatch between  $\text{Cr}_2\text{O}_3$  and Si alone but could be indicative of an increasing degree of densification as the temperature increases, compensating for the effects of thermal expansion mismatch. The stress changes by approximately 186 MPa, becoming significantly more tensile, over the range from 185 °C to 375 °C, and then drops sharply to close to its initial value from 375 °C to 500 °C. This suggests that 375 °C marks the end of densification and the start of grain growth, with thermal expansion mismatch driving the development of more compressive stresses. [13] On cooling, the stress varies approximately by the amount expected due to thermal expansion mismatch. However, given the continued increasing crystallinity up to 1000 °C, as indicated by the x-ray diffraction data, it is unlikely that the material is in its fully equilibrium state at 500 °C.

Long-term measurements of stress in as-deposited films (Figure 1(d)) show that even at room temperature, the film stress changes over time. In this case, the films become more compressive, with the stress changing by up to 84 MPa more compressive *versus* the initial value over the course of 1.46 years. This effect appears to largely independent of film thickness and deposition conditions.

### 3.2. Surface Roughness

Surface roughness (root-mean-square and arithmetic mean) was measured by atomic force microscopy (AFM) using a tip of nominal end radius 7 nm. As Figure 2 shows, the roughness appears to trend slowly upwards with increasing film thickness, and possibly with increasing power. However, even for film thicknesses of 900 nm the roughness is still  $\approx 3$  nm. This small increase could be due in increasing film thickness. For comparison, typical values for wet-oxidation grown  $\text{SiO}_2$  and low-stress low-pressure chemical vapor deposited  $\text{SiN}_x$  are  $< 1$  nm and 2 nm to 5 nm, respectively, for films  $\sim 100$  nm thick. We also looked the surface roughness with AFM after heating to 1000 °C, shown in figure S2. The the roughness increased to 13nm. This increase in roughness is consistent with the crystallization observed with XRD and later with TEM.

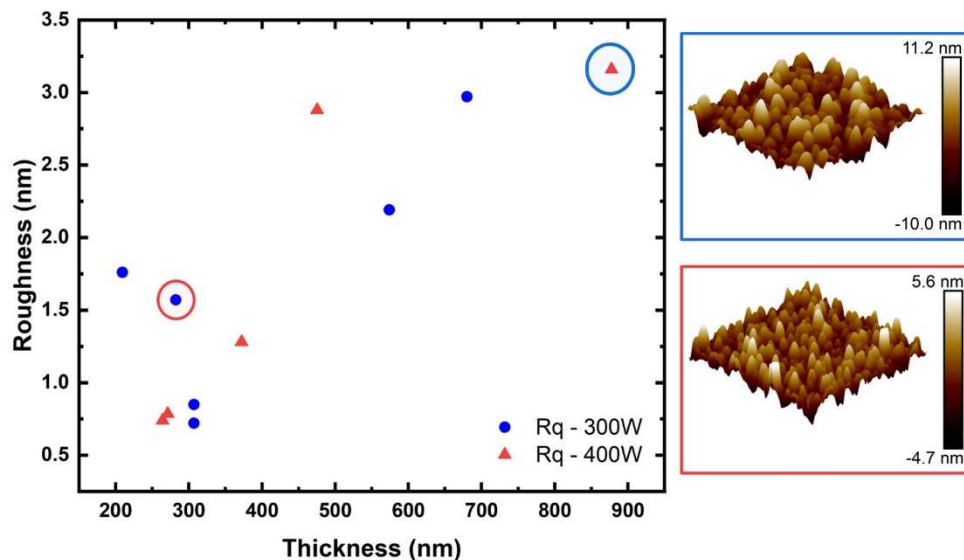


Figure 2. Film root-mean-squared roughness,  $R_q$ , as a function of thickness for chromium oxide films deposited using 6.7 Pa to 7.2 Pa of Ar working gas pressure and deposition power of 300 W and 400 W. The insets are atomic force microscope images of the data points indicated.

### 3.3. Wet Etch Rate

Chromium oxide etches in ceric ammonium nitrate etchants. In contrast to Cr metal, which etches in a well-controlled fashion, we find that our chromium oxide films exhibit an incubation time before etching begins and appears to etch preferentially from edges. The reason for this behavior is unknown. An analysis by x-ray photoelectron spectroscopy did not provide any evidence for a difference in composition or oxidation state between the film surface and the bulk. These characteristics preclude the use of these films as a wet-etch patternable masking material. However, chromium oxide is an excellent sacrificial layer material and can act as an etch stop for a variety of wet etch chemistries. We checked chrome oxide against other wet chemistries such as HF (49%), BOE (6:1), SC1 (H<sub>2</sub>O:NH<sub>4</sub>OH:H<sub>2</sub>O<sub>2</sub> 5:1:1, [NH<sub>4</sub>OH] = 29 % by mass, [H<sub>2</sub>O<sub>2</sub>] = 30 % by mass), SC2 (H<sub>2</sub>O:NH<sub>4</sub>OH:HCl 5:1:1, [H<sub>2</sub>O<sub>2</sub>] = 30 % by mass, [HCl]=37 % by mass) baths, and sulfuric acid/peroxymonosulfuric acid/hydrogen peroxide solution. Chrome oxide was found to be resistance to all the mentioned chemistries.

In order to investigate its utility as a sacrificial layer for forming micro- and nanoscale channels, we fabricated a series of long lines of chromium oxide, encapsulated in low-stress SiN<sub>x</sub>, using sputter deposition and lift-off with a bilayer resist, consisting of Lift Off Resist (LOR) under a standard i-line (diazonaphthoquinone/novolak) resist. Etch rate as a function of line size and time is displayed in Figure 3(a). A reaction diffusion model [14] was used to fit the data using the Levenberg Marquardt method. The model was modified to add a delay to represent the incubation time that was observed. The equation is as follows

$$l = -\frac{D}{k} + \sqrt{\left(\frac{D}{k}\right)^2 + MD(t - de)} \quad \text{Equation 1}$$

Where  $l$  is the lateral etch distance,  $D$  is the diffusivity,  $k$  is the reaction rate constant,  $M$  is a constant,  $t$  is the time, and  $de$  is the incubation time. The derived diffusivity and reaction rate constants for each fit are shown in the insert.

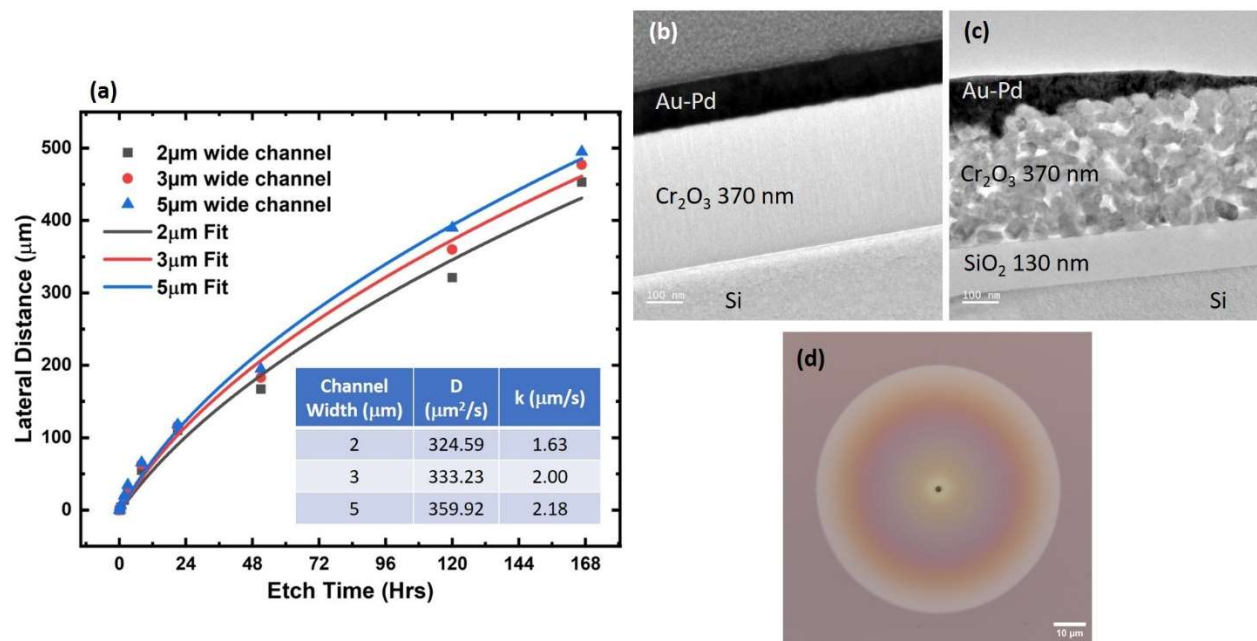


Figure 3. (a) Lateral etch distance as a function of time for encapsulated  $\text{Cr}_2\text{O}_3$  lines of 2  $\mu\text{m}$ , 3  $\mu\text{m}$ , and 5  $\mu\text{m}$  width, and 230 nm, 280 nm and 360 nm thickness respectively. The resulting diffusivities and reaction rate constants are shown in the insert. TEM images of (b) as deposited  $\text{Cr}_2\text{O}_3$  film and (c) after annealing at 1000°C. The as deposited film appears amorphous, and the annealed films is more crystalline confirming the XRD data. (d) Radial etch pattern from a 1 $\mu\text{m}$  hole in a capping layer.

In some instances, it is desirable for a sacrificial layer to etch with a high degree of uniformity, for example to enable the creation of a suspended circular membrane. Such behavior may be anticipated if the sacrificial material is amorphous. The as-deposited chromium oxide is amorphous, as indicated by x-ray diffraction and confirmed by TEM in Figure 3(b-c). The etch characteristics for this type of application were explored by creating holes  $\approx 1 \mu\text{m}$  in diameter in a capping film and imaging the resulting etch pattern after different periods of time. An example is shown in Figure 3(d). Chromium oxide etched radially and uniformly from the hole.

### 3.4. Dry Etching

Chromium oxide is etched in a  $\text{Cl}_2/\text{O}_2$  chemistry [15]. Etching was performed with an inductively coupled plasma (ICP) in a reactive ion etch system. The  $\text{Cl}_2$  and  $\text{O}_2$  flows adjusted to give an  $\text{O}_2$  concentration of 16%. The ICP power was 1200W and the DC 6W. The temperature was set to 50°C. Pressure was set to  $\approx 1.6 \text{ Pa}$  (12mTorr). The resulting chemical reactions leads to the formation of  $\text{CrO}_2\text{Cl}_2$ , which is volatile above -90°C, resulting in a clean etch without any residues (Figure 4). Photoresist was patterned and used a mask to etch the chromium oxide. The etch rate was monitored using ellipsometry. The etch rate under these conditions was found to be approximately 80 nm/min.

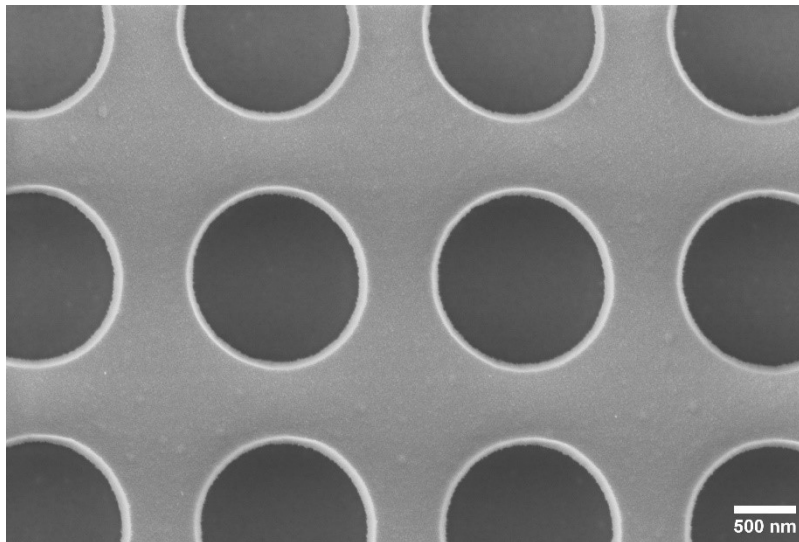


Figure 4 Dry etched 1.2 micrometer diameter holes in chromium oxide. The holes exhibit a clean etch without any residues. The resist was striped prior to imaging.

### 3.5. Ion Milling

The milling rate for  $\text{Cr}_2\text{O}_3$  at varying angles was measured, as graphed in Figure 5a. The argon ion flux was 0.43  $\text{mA}/\text{cm}^2$  and the incident energy was 200 eV. Angles were varied from 90 deg to 135 deg to the ion beam. The rate increase with increasing angles. Figure 5b shows the milling rate at 90 deg for varying materials.  $\text{Cr}_2\text{O}_3$  has one of the lowest rates, suggesting it would make a good hard mask. This holds even for large angles, which have rates less than 10 nm/min.

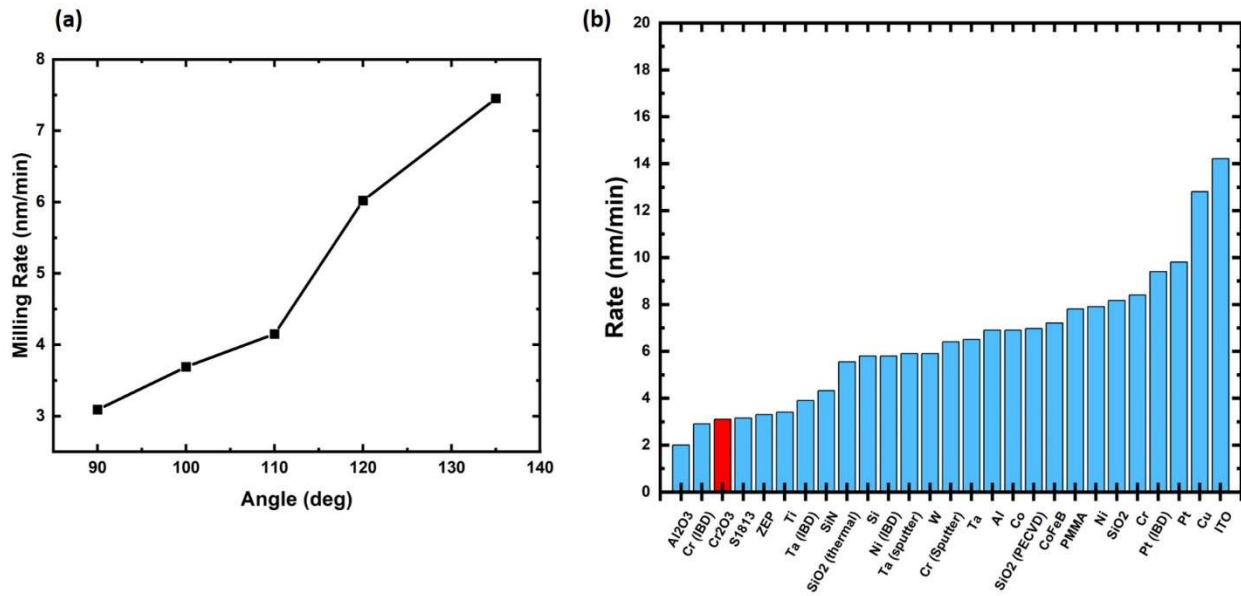


Figure 5 (a) Ion milling rate at varying angles. (b) Ion milling rate of various materials.  $\text{Cr}_2\text{O}_3$  is highlighted in red.

### 3.6. Hard Mask/Pattern Transfer

For a material to be a good hard mask, it must have both a low etch rate and allow for good pattern transfers.  $\text{Cr}_2\text{O}_3$  does not etch in fluorine-based chemistries. Combined with its low milling rate,  $\text{Cr}_2\text{O}_3$  meets the first criterion. To study pattern transferability, lines were lithographically patterned in i-line photoresist and hydrogen silsesquioxane (HSQ). The exposed  $\text{Cr}_2\text{O}_3$  was dry etched as described above. Scanning electron micrographs of the results are shown in Figure 6. The etch exhibits minimal undercut. The slope of the etched  $\text{Cr}_2\text{O}_3$  lines follows that of the resist. The pattern is faithfully transferred from the resist to  $\text{Cr}_2\text{O}_3$ , which can later be used as a hard mask.

To demonstrate pattern transfer, 75nm low stress nitride was reactive-ion etched with a  $\text{CF}_4$  chemistry (Figure 6(c)) using a 50nm chromium oxide hard mask. The sample was over etched by 55%, resulting in etching of the Si wafer and allowing for some “grass” growth. An optimized etch could reduce the formation of the grass by limiting the etching of the Si. The etch rate of chromium oxide was found to be  $\sim 6$  nm/min while nitride was 48nm/min. Chromium oxide was also tested as a mask for deep reactive ion etching (DRIE) of silicon using a Bosch process (Figure 6(d)). A 100nm chromium oxide layer was patterned with features sizes between 1.2  $\mu\text{m}$  and 10  $\mu\text{m}$ . 100 loops of etching/deposition steps were used to etch the Si. Given the small feature sizes, 20 loops resulted in the erosion of Si just under the chromium oxide layer. The white lines observed on the sidewalls are excess polymer from the extended etching. The thin 100 nm chromium oxide layer can be seen as a thin line above the silicon layer. No significant amount of  $\text{Cr}_2\text{O}_3$  was etched during the process. We also etched large features (500  $\mu\text{m}$  to 1 mm) using the chromium oxide as a mask. After etching 350  $\mu\text{m}$  of Si, we still could not measure any significant loss of thickness in the chromium oxide layer. Chromium oxide’s excellent selectivity makes it ideal as a stop layer for DRIE of Si. It is particularly useful when forming membranes by deep etching through a wafer to release a surface film. We have been successful in etching through a 400 $\mu\text{m}$  wafer and stopping on 40nm of chromium oxide to create SiN membranes.

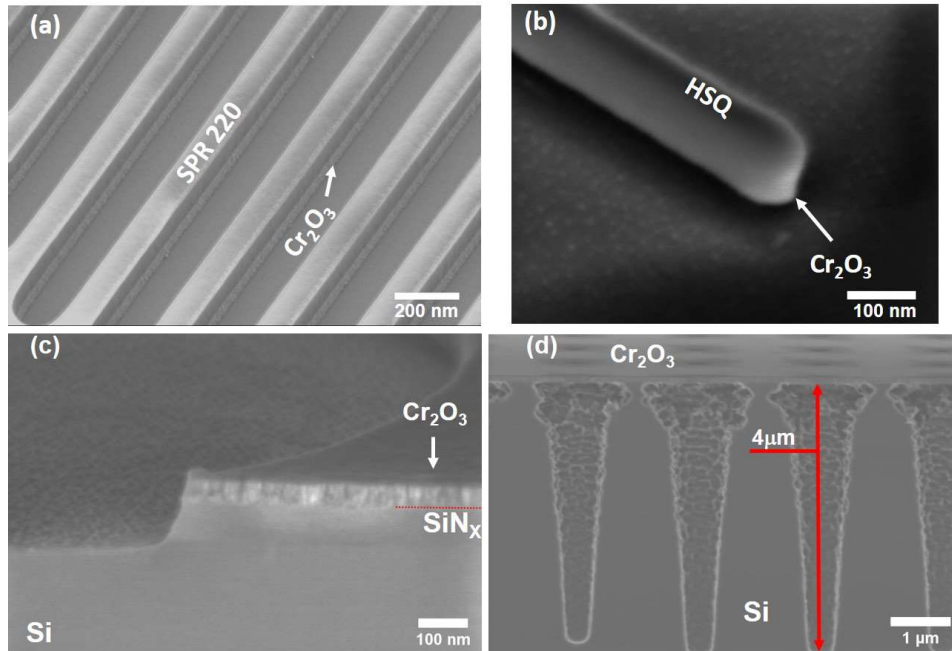


Figure 6. Patterned chromium oxide. (a) 430 nm lines formed with a photoresist mask. (b) 20 nm line patterned using an HSQ mask. Pattern transfer using chromium oxide as a hard mask. (c) Low-stress silicon nitride etched using a 50nm chromium oxide mask. (d) Si deep etch using a Bosch process with a 100 nm thick chromium oxide mask. Feature size is 1.2  $\mu\text{m}$

#### 4. Discussion/Conclusions

Chromium oxide is an ideal sacrificial layer material – robust, chemically inert, readily patternable into precise geometries, yet easy to remove in a highly controlled fashion using both wet and dry etches. Employed as a sacrificial layer, chromium oxide permits the reliable fabrication of devices for micro- and nanofluidic applications. The introduction of chromium oxide into device process flow will have a profound impact on fabrication of both MEMS and NEMS, where removal of large area of a sacrificial material is required. This is typically done using silicon dioxide as a sacrificial material and vapor hydrofluoric acid (HF) to selectively etch it. Chromium oxide provides an exciting alternative because its etch chemistry is orthogonal to that of most common materials used in MEMS device fabrication. It therefore enables the use of a wide range of materials that are not compatible with HF, and, because of its effectively infinite etch selectivity, supports the fabrication of unique device geometries with very large undercuts. In addition, the fact that it is chemically inert with respect to most materials, even at high temperatures, opens up the possibility of using it as an encapsulant to protect complex and delicate structures during processing, thus increasing thermal budgets and enabling simpler process flows. Given its many advantageous properties, we believe that chromium oxide will rapidly take its place as a standard and versatile element in many device fabrication processes. We have therefore endeavored to provide a comprehensive set of experimental data that will enable the interested researcher to rapidly converge on an optimized process for their specific application.

## Acknowledgments

Research performed in part at the NIST Center for Nanoscale Science and Technology.

## References

- [1] B.A. Peeni, M.L. Lee, A.R. Hawkins, A.T. Woolley, Sacrificial layer microfluidic device fabrication methods, *ELECTROPHORESIS* 27(24) (2006) 4888-4895.
- [2] K. Winchester, S.M.R. Spaargaren, J.M. Dell, The use of ZnS as a sacrificial layer in the construction of PECVD SiN/sub x/ self-supporting structures, *IEEE*, 1998.
- [3] P. Pal, K. Sato, Various shapes of silicon freestanding microfluidic channels and microstructures in one-step lithography, *Journal of Micromechanics and Microengineering* 19(5) (2009) 055003.
- [4] I. Yanagi, T. Ishida, K. Fujisaki, K.-I. Takeda, Fabrication of 3-nm-thick Si<sub>3</sub>N<sub>4</sub> membranes for solid-state nanopores using the poly-Si sacrificial layer process, *Scientific Reports* 5(1) (2015) 14656.
- [5] M. Tanase, J. Winterstein, R. Sharma, V. Aksyuk, G. Holland, J.A. Liddle, High-Resolution Imaging and Spectroscopy at High Pressure: A Novel Liquid Cell for the Transmission Electron Microscope, *Microscopy and Microanalysis* 21(6) (2015) 1629-1638.
- [6] W. Sparreboom, J.C.T. Eijkel, J. Bomer, A. Van Den Berg, Rapid sacrificial layer etching for the fabrication of nanochannels with integrated metal electrodes, *Lab on a Chip* 8(3) (2008) 402.
- [7] T.-G. Wang, Y. Liu, H. Sina, C. Shi, S. Iyengar, S. Melin, K.H. Kim, High-temperature thermal stability of nanocrystalline Cr<sub>2</sub>O<sub>3</sub> films deposited on silicon wafers by arc ion plating, *Surface and Coatings Technology* 228 (2013) 140-147.
- [8] K.R. Williams, K. Gupta, M. Wasilik, Etch rates for micromachining processing-part II, *Journal of Microelectromechanical Systems* 12(6) (2003) 761-778.
- [9] E. Chason, Stress Measurement in Thin Films Using Wafer Curvature: Principles and Applications, in: S. Schmauder, C.-S. Chen, K.K. Chawla, N. Chawla, W. Chen, Y. Kagawa (Eds.), *Handbook of Mechanics of Materials*, Springer Singapore, Singapore, 2019, pp. 2051-2082.
- [10] V. Guilbaud-Massereau, A. Celerier, J. Machet, Study and improvement of the adhesion of chromium thin films deposited by magnetron sputtering, *Thin Solid Films* 258(1-2) (1995) 185-193.
- [11] X. Pang, K. Gao, A.A. Volinsky, Microstructure and mechanical properties of chromium oxide coatings, *Journal of Materials Research* 22(12) (2007) 3531-3537.
- [12] D. Ritu, Synthesis and Characterization of Chromium Oxide Nanoparticles, *IOSR Journal of Applied Chemistry* 8(3) (2015) 05-11.
- [13] G. Abadias, E. Chason, J. Keckes, M. Sebastiani, G.B. Thompson, E. Barthel, G.L. Doll, C.E. Murray, C.H. Stoessel, L. Martinu, G. M., C. C., C. J., G. J., Review Article: Stress in thin films and coatings: Current status, challenges, and prospects, *Journal of Vacuum Science & Technology A* 36(2) (2018) 020801
- [14] D.J. Monk, D.S. Soane, R.T. Howe, Hydrofluoric Acid Etching of Silicon Dioxide Sacrificial Layers: II . Modeling, *Journal of The Electrochemical Society* 141(1) (1994) 270-274.
- [15] H. Ekinici, N.M.S. Jahed, M. Soltani, B. Cui, The Role of Oxygen on Anisotropy in Chromium Oxide Hard Mask Etching for Sub-Micron Fabrication, *IEEE Transactions on Nanotechnology* 20 (2021) 33-38.